T. Makkonen, T. Pensala, J. Vartiainen, J. V. Knuuttila, J. Kaitila, and M. M. Salomaa, "Estimating materials parameters in thin-film BAW resonators using measured dispersion curves", IEEE Transactions on Ultrasonics, Ferroelectrics, and Frequency Control, Vol. 51, No. 1, pp. 42–51, January 2004.

Estimating Materials Parameters in Thin-Film BAW Resonators Using Measured Dispersion Curves

Tapani Makkonen, *Member, IEEE*, Tuomas Pensala, Juha Vartiainen, Jouni V. Knuuttila, Jyrki Kaitila, and Martti M. Salomaa, *Member, IEEE*

***Abstract*—The dispersion curves of Lamb-wave modes propagating along a multilayer structure are important for the operation of thin-film bulk acoustic wave (BAW) devices. For instance, the behavior of the side resonances that may contaminate the electrical response of a thin-film BAW resonator depends on the dispersion relation of the layer stack. Because the dispersion behavior depends on the materials parameters (and thicknesses) of the layers in the structure, measurement of the dispersion curves provides a tool for determining the materials parameters of thin films. We have determined the dispersion curves for a multilayer structure through measuring the mechanical displacement profiles over the top electrode of a thin-film BAW resonator at several frequencies using a homodyne Michelson laser interferometer. The layer thicknesses are obtained using scanning electron microscope (SEM) measurements. In the numerical computation of the dispersion curves, the piezoelectricity and full anisotropy of the materials are taken into account. The materials parameters of the piezoelectric layer are determined through fitting the measured and computed dispersion curves.**

I. Introduction

Thin-film bulk acoustic wave (BAW) devices first appeared two decades ago [1], [2], but only recently their large-scale commercial applications have been introduced [3]. This is because of the considerable technical difficulties in obtaining consistently high-quality, thin-film piezoelectric layers with uniform thickness and the problems in the suppression of the side resonances that may contaminate the frequency response close to the main resonance. For the behavior of the side resonances, the dispersion characteristics of the Lamb-wave modes propagating along a layered structure are important. In addition, many modeling techniques for thin-film BAW devices, such as the mode-matching method [4], require knowledge of the dispersive behavior. This may be computed numerically or, alternatively, the measured dispersion curves can be used in the model.

Manuscript received June 18, 2002; accepted July 14, 2003. This research has been funded by Nokia Mobile Phones Ltd, Salo, Finland.

T. Makkonen, J. Vartiainen, J. V. Knuuttila, and M. M. Salomaa are with the Materials Physics Laboratory, Helsinki University of Technology, P.O. Box 2200 (Technical Physics), FIN-02015 HUT, Helsinki, Finland (e-mail: tapani@focus.hut.fi).

T. Pensala and J. Kaitila are with the Technical Research Centre of Finland (VTT), P.O. Box 1208, FIN-02044 VTT, Espoo, Finland (e-mail: tuomas.pensala@vtt.fi).

In this paper we obtain the dispersion curves using laser-interferometric probing and subsequent Fourier-transformation techniques, a procedure also reported in [5] and [6]. The mechanical displacements on the top surface of a solidly mounted thin-film BAW resonator are measured, and the spatial amplitude data obtained is Fourier transformed to find the lateral component of the wavevector for the modes excited at each frequency [5]. This approach also allows for an evaluation of the materials parameters of thin films through fitting the experimental dispersion curves to those computed numerically using matrix techniques. It should be noted that the materials parameters of a thin film may be different from those of bulk material; the materials parameters also provide information on the quality of the film. The experimentally determined materials parameters can be used in the simulations of thin-film BAW resonators and filters to predict their behavior more accurately and reliably.

We present the numerically computed dispersion curves together with those obtained experimentally. The materials parameters used in the computation are optimized to yield matching between the measured and computed dispersion curves. The shortcomings and benefits of this approach for determining the materials parameters are discussed.

II. Layer Stack and Solidly Mounted Resonator

A. Description of the Resonator

The cross section of our solidly mounted thin-film resonator (SMR) is shown in Fig. 1. The piezoelectric material is zinc oxide (ZnO) sandwiched between a molybdenum (Mo) bottom electrode and an aluminum (Al) top electrode. In the measured SMR, only the topmost Al layer is patterned to form the top electrode; the floating bottom electrode is capacitively connected to the large-area ground plane surrounding the top electrode. The layers between the glass substrate and the bottom electrode constitute the acoustic mirror used to prevent leakage of the acoustic wave into the substrate. These layers operate as a Bragg reflector in which the acoustic wave is strongly reflected at each materials interface. The layer thicknesses within the acoustic mirror are chosen such that the phases of the reflected waves interfere appropriately.

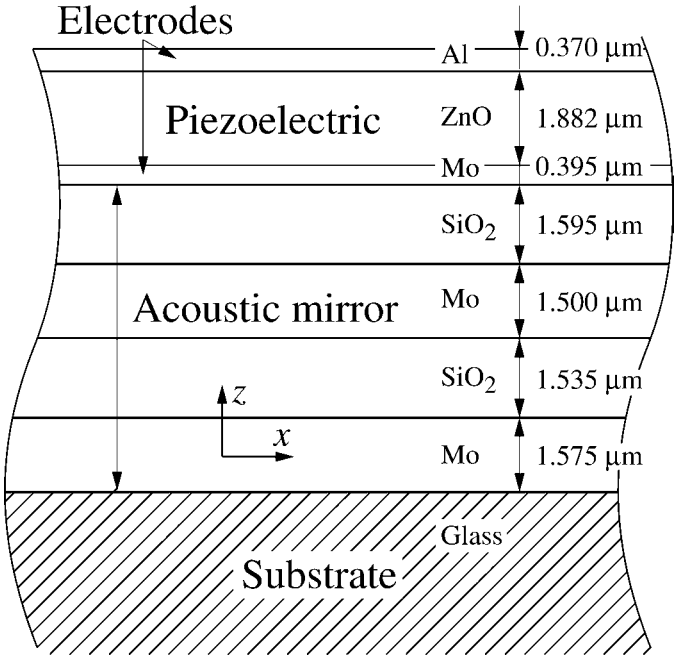

Fig. 1. Solidly mounted composite thin-film BAW resonator (SMR) configuration. Two Mo-SiO_2 layer pairs form the acoustic mirror, which acoustically isolates the active region of the resonator from the substrate. The layer thicknesses were determined at several different locations along the layer interfaces using SEM; the thickness values shown are averaged.

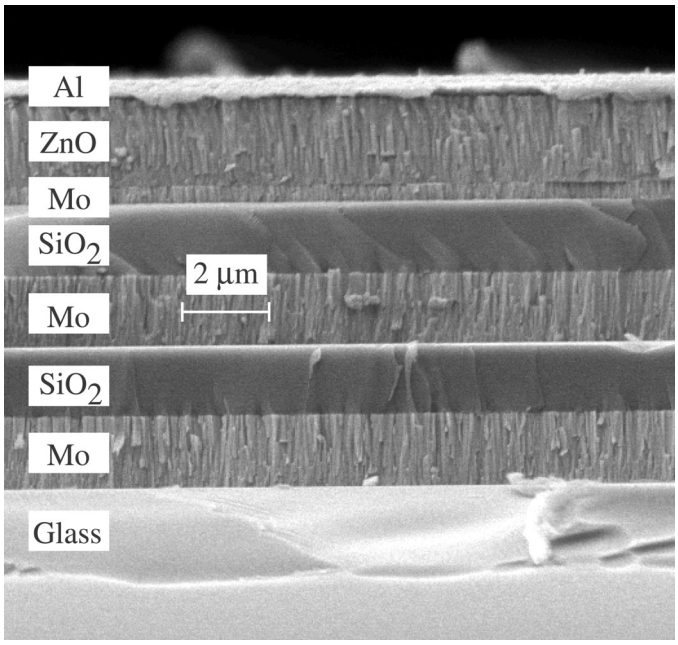

Fig. 2. SEM image of the cut cross section of the SMR stack, used to determine the layer thicknesses. The columnar structure of the Mo and ZnO films is clearly visible.

The higher the difference between the acoustic impedances of the materials, the more effectively the mirror operates. The acoustic mirror can be used to transform the acoustic impedance[1] of the substrate, such that the interface between the bottom electrode and the acoustic mirror for the chosen wave mode appears either free or clamped. The SMR considered here is a $\lambda/2$ mode configuration [8], in which the first layer in the acoustic mirror (below the bottom electrode) is the one with the lower acoustic impedance, and the thickness of the piezoelectric layer is approximately half a wavelength at the fundamental resonance frequency. In this configuration, the interface between the bottom electrode and the acoustic mirror appears free.

B. Fabrication Procedure

The resonator layer stack was fabricated on a 100-mm diameter glass substrate (Corning C7059, Corning Glass Works, Corning, NY). Metal layers (Mo, Al) were all direct current (DC) sputtered. A silane-based, plasma-enhanced chemical vapor deposition (PECVD) process was used to deposit SiO_2 for the low acoustic impedance reflector layers. The ZnO piezoelectric layer was radio frequency (RF) sputtered from a ZnO target in an oxygen atmosphere. The top Al electrode was the only patterned layer. This was done using standard lithography and a wet etch having a high selectivity against the rather sensitive ZnO.

[1]The acoustic impedance Z for a wave mode with phase velocity v propagating in a medium with density ρ is defined as $Z = \rho v$ [7].

III. Measurements

A. Measuring Layer Thicknesses Using Scanning Electron Microscopy

A cross section of the wafer was prepared in order to check the layer thicknesses. The wafer was sliced using a glass cutter because standard sawing would result in an excessively rough surface for the cross section. The cut is located on the wafer only a few millimeters away from the resonator used in the interferometric imaging. Hence, the layer thicknesses in the two are expected to differ only slightly.

The layer thicknesses were determined using scanning electron microscopy (SEM) equipment (Model Leo 1560, LEO Electronenmikroscopie GmbH, Oberkochen, Germany). A SEM image of the layer stack is shown in Fig. 2. The top Al electrode edge was strongly deformed in the slicing (see Fig. 2), but its thickness could be measured with a profilometer from the etched patterns.

B. Laser-Interferometric Probing of Vibration Amplitude

For interferometric measurements, the SMR was driven at 195 selected frequencies within the range from 100 MHz to 2220 MHz. In the measurement setup, the optical scanning interferometer sweeps the sample surface at each frequency, recording two quantities for each (x, y) point, the time-averaged amplitude of the vertical motion of the surface and the intensity of the reflected light. The selected scanning area is a 231×231 micrometer square consisting of 350×350 points. Hence, the spatial scanning step is 0.66 μm.

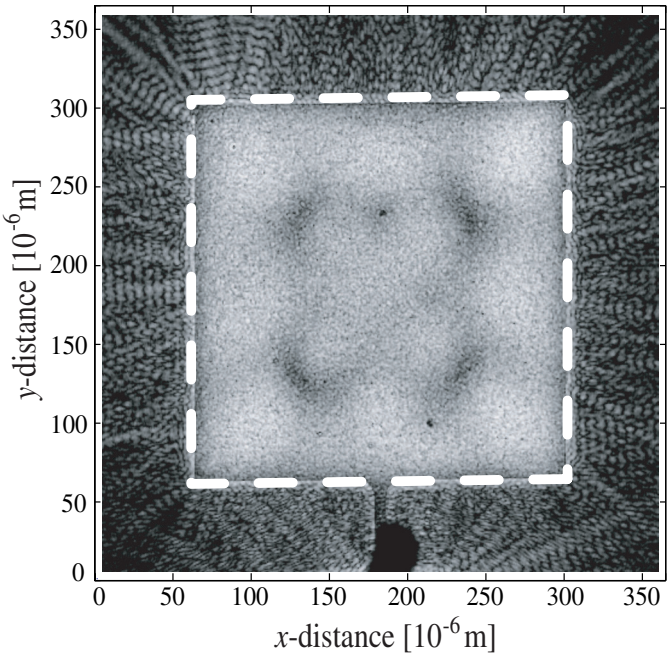

Fig. 3. Measured magnitudes of displacement components in the z-direction at the top surface of the SMR at the frequency 1030 MHz. Lighter shades indicate larger values. The area measured with the laser probe at each frequency (over which the 2-D FFT is carried out) is indicated with the dashed line. The end of a bond wire is seen in the middle of the bottom part of the figure.

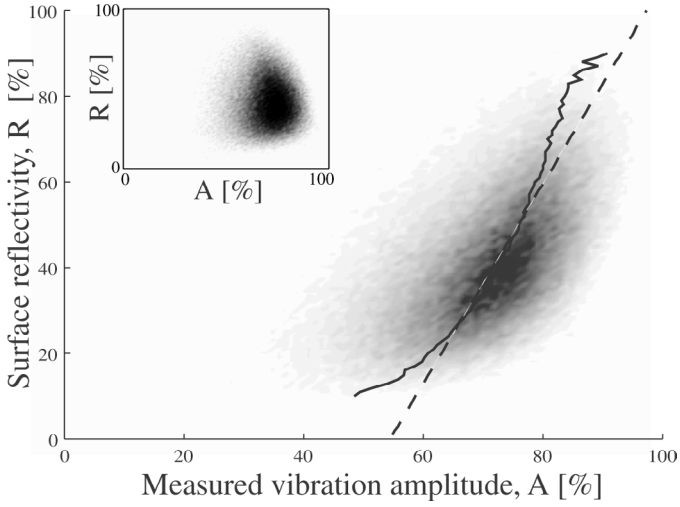

Fig. 4. Raw data for the number of measurement points possessing the same vibration amplitude-reflectivity (A, R) values, without any corrections applied. The darker shades of gray indicate a larger number of measured points. The center-of-mass value of the vibration-amplitude distribution for each reflectivity (solid line) and a line fitted to this curve (dashed line) also are plotted. The increase in the variation of the center-of-mass value versus reflectivity when approaching toward higher and lower reflectivities is due to the decreasing number of (A, R) pairs in these directions. The inset displays the number of points for each vibration amplitude-reflectivity pair after application of the correction procedure.

Fig. 3 presents the measured magnitudes of the displacement component in the z-direction at the frequency 1030 MHz. The long-wavelength modes are visible in the amplitude data, even for the bare eye. They are caused by the finite size of the resonator; waves associated with the fundamental thickness-extensional (TE1) mode that propagates along the lateral direction in the layered structure are reflected at the edges of the top electrode, and a standing-wave pattern is formed. At the frequency of the measurement, the TE1 mode is trapped into the electroded region and the wave amplitude decays exponentially outside the top electrode. Waves propagating in the lateral direction occur in a structure with finite lateral dimensions, but they are not present in an ideal structure with infinite extent. Our technique for experimentally determining the dispersion curves relies on the presence of the edges, such that standing-wave patterns (eigenmodes) due to waves having finite lateral component of wavevector are formed.

Due to the different reflectivities of the metallized and nonmetallized regions, there is a step discontinuity in the measured vibration amplitude at the boundary of the top electrode. The signal level of the interferometer also varies pointwise owing to surface roughness. The measured vibration amplitude A_{meas} depends on the reflectivity R of the surface:

$$A_{\mathrm{meas}}(x, y) = A_{\mathrm{meas}}(A_{\mathrm{t}}(x, y), R_{\mathrm{t}}(x, y)), \qquad (1)$$

where $A_{\mathrm{t}}(x, y)$ and $R_{\mathrm{t}}(x, y)$ are the actual vibration amplitude and surface reflectivity at the location (x, y), respectively. The signal-to-noise ratio is increased by compensating the spatial variations in the reflectivity (within the area of the top electrode), caused by the roughness of the sample surface. Here, it is assumed that the roughness is uniform, i.e., the spatial distribution of the points with a given reflectivity within the top-electrode surface is uniform. In addition, we used a heuristic model to approximate (1):

$$A_{\mathrm{meas}}(x, y) = A(x, y) - k[1 - R_{\mathrm{meas}}(x, y)], \qquad (2)$$

where R_{meas} is the measured relative reflectivity scaled into the range $[0, 1]$ and $A(x, y)$ is the corrected amplitude approximating the true amplitude A_{t}. This linear relation essentially expresses the fact that, for constant true vibration amplitude, the measured amplitude decreases with decreasing surface reflectivity R_{t}. The coefficient k in (2) is determined from the vibration amplitude-reflectivity (A–R) distribution as described below.

The number of measurement points possessing the same measured vibration amplitude-reflectivity values are counted to obtain the A–R distribution plotted in Fig. 4. Then, the center of mass of the vibration-amplitude distribution for each reflectivity R is determined [here denoted as $U_0(R)$]. The curve $U_0(R)$ is indicated in Fig. 4 as the solid line. Were the reflectivity and vibration amplitude independent, the center-of-mass value and the width of the amplitude distribution would be equal for all values of the reflectivity. Next, a line (the dashed line in Fig. 4) is fitted to the $U_0(R)$ curve in the region of the distribution containing the largest number of points. Using the equation for the fitted line allows us to estimate k in (2), from

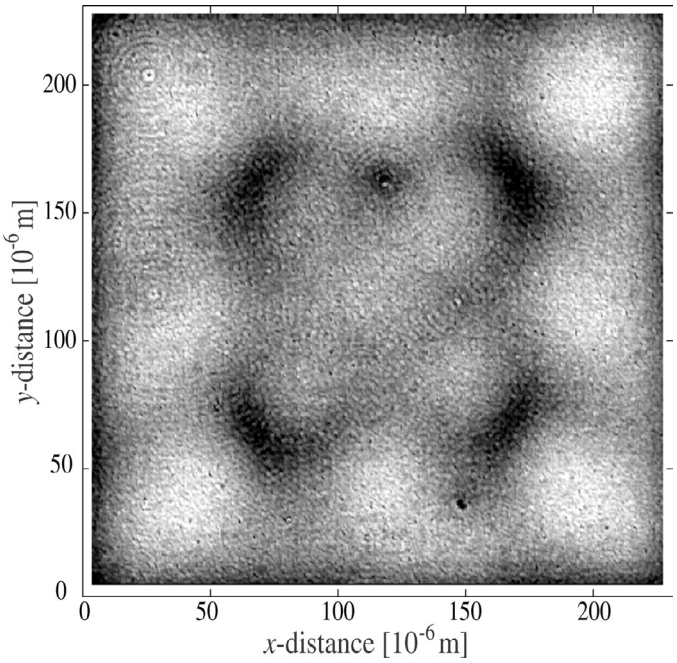

Fig. 5. Vibration-amplitude profile after the procedure for reducing the influence of variations in surface reflectivity is applied. Lighter shades indicate larger amplitude. Note the surface imperfections acting as scattering centers for the acoustic waves.

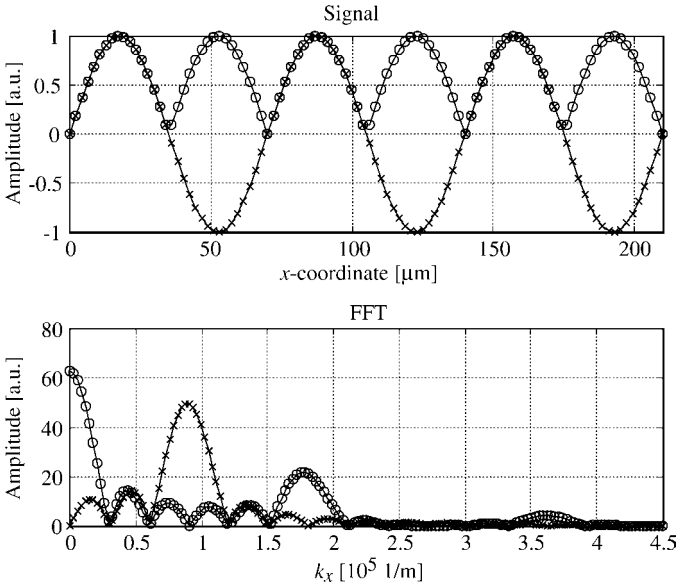

Fig. 6. Top: Sine signal representing the actual vibration amplitude of the surface (crosses) and its magnitude representing the signal measured by the interferometer (circles). Bottom: FFT of the two signals in the top figure.

which the corrected vibration amplitude is solved at each scanning point in terms of the measured quantities A_{meas} and R_{meas}.

The inset in Fig. 4 shows the A–R distribution obtained after the correction procedure is applied. The corresponding resulting profile of surface deflection after the correction procedure is shown in Fig. 5. It can be seen that the amount of discernible detail has increased, e.g., one may see circular waves scattered by imperfections.

C. Measured Dispersion Curves

In the ideal case, the eigenmodes correspond to sinusoidal waves, and Fourier analysis may be applied to study the excitation spectrum of the surface modes. However, the actual nonideal shape of the resonator, its absolute size, and the imperfections on the sample surface may affect the eigenmodes. In order to study these effects, we measured two resonators (located close to each other on the wafer) with identical layer structure but having different top electrode areas. The excitation spectra for the two were identical. It may be concluded that the influence of the size of the resonator, as well as edge effects, are negligible.

The effects due to our interferometer measuring only the magnitude of the vibration amplitude are illustrated in Fig. 6 for a one-dimensional (1-D) case. In the fast Fourier transform (FFT) of the $|\sin(x)|$ signal, peaks due to the DC component (at $k_x = 0$) and higher harmonics appear (the first one of these higher harmonics is close to $k_x = 3.6 \times 10^5$ 1/m). The harmonic content also may be increased due to the resonator operating in the nonlinear region because of high input power. However, the largest input power used in the measurements (20 dBm) is low enough that the operation of the resonator is linear. It also is seen in Fig. 6 that the wavelength is obtained as $\lambda = 2 \times (2\pi/k_x)$, where k_x is the wavenumber determined from the FFT of the $|\sin(x)|$ function. Hence, the Fourier transform enables one to study spatial waves with wavelengths larger than the Nyqvist limit, i.e., $\lambda = 4\times$ scanning step $= 4 \times 0.66$ μm $= 2.6$ μm. Owing to the finite size of the scanned area (side length L), the smallest observed wavenumber is on the order of $k_x = \pi/L$, corresponding to the wavelength $\lambda \approx 2L \approx 460$ μm.

In the 2-D FFT applied to the corrected amplitude data, the symmetric Hanning window function $w(x, y) = \sin^2(\pi x/L)\sin^2(\pi y/L)$ is applied, where L is the width of the sampling window. The effect of using this window function can be seen by comparing Figs. 6 and 7. Usage of the window function suppresses the side peaks but broadens the width of the main peak. This is because the FFT of the window function used has a somewhat wider main lobe, but stronger suppression of the side peaks in comparison with the FFT of a step function.

A typical result obtained by carrying out 2-D FFT on the measured vibration amplitudes, is shown in Fig. 8. There is no angular dependence in the lateral wavenumber k on the surface, because the ZnO is rather well c-axis oriented (see Fig. 2), consequently, it is isotropic in the plane of the film. Hence, angular integration (averaging) in the k space can be used to reduce noise and to sample all the modes at a given wavelength [5] (the integration path is a circle, centered at the origin). The resulting k spectrum is shown in Fig. 9. The sensitivity of the interferometer is sufficiently high to allow for weakly excited modes to be detected. Repeating the process and plotting the k spectrum for all the frequencies studied yields the dispersion curves shown in Fig. 10.

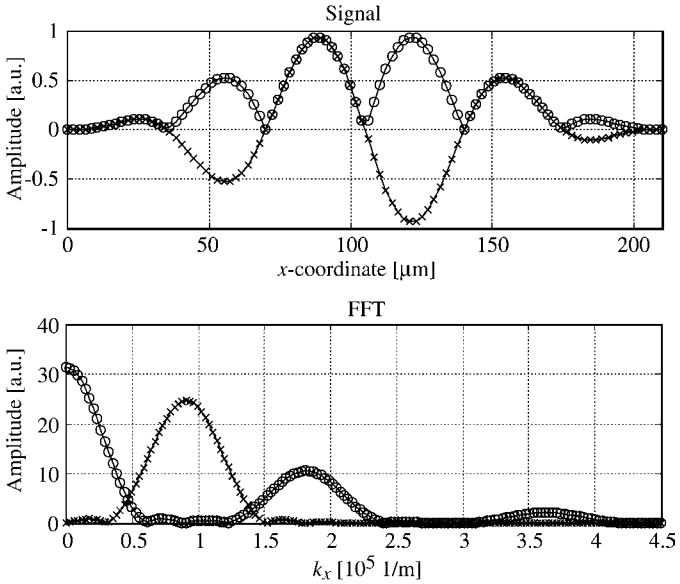

Fig. 7. Top: Sine signal representing the actual vibration amplitude of the surface (crosses) and its magnitude representing the signal measured by the interferometer (circles), both multiplied by the window function $\sin^2(\pi x/L)$, where L is the width of the sampling window (here 210 μm). Bottom: FFT of the two signals in the top figure.

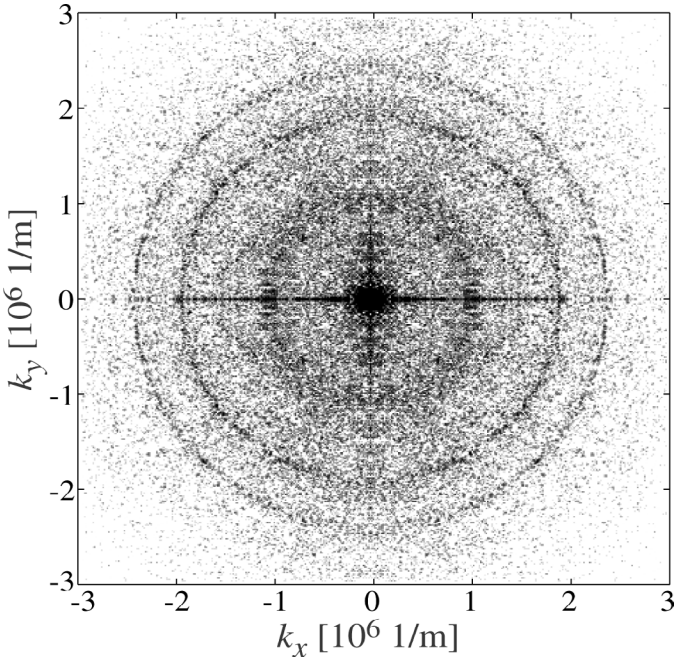

Fig. 8. Two-dimensional FFT of the measured vibration amplitudes at the frequency 1029 MHz.

A measurement of the phase of the vibration is not required for the determination of the dispersion curves, although lack of the phase data in our system limits the largest observable lateral wavenumber. Interferometer setups that also enable the measurement of the phase information were recently presented [9].

IV. Simulations

The dispersion curves are computed using matrix techniques, accommodating anisotropic and piezoelectric layers [10]. A numerically robust global matrix method [11] is used in the implementation that properly handles the exponentially increasing/decreasing field amplitudes within the layers. Recently, a scattering-matrix approach, which also avoids the numerical instabilities encountered in the transfer-matrix method, has been proposed in [12]. In the matrix formulation used here, straight-crested waves are considered, i.e., the field quantities are taken to be independent of one of the directions, say, the y-direction. The fields are taken to assume the form $e^{-ik_x x - ik_z z} e^{i\omega t}$, where ω is the angular frequency and k_x and k_z are the x- and z-components of the wavevector. Substituting this Ansatz into the constitutive and governing equations for the piezoelectric material under the quasistatic approximation, eight bulk-wave modes in an infinite piezoelectric medium are obtained. Imposing boundary conditions at the materials interfaces for the mechanical x-, y-, and z-displacements, the electric potential, the stress components zx, zy, and zz, and the z-component of electric displacement, the equations describing the complete layered structure are obtained. The model used also allows taking into account the vacuum half-space (which supports only electric fields) on top and/or bottom of the stack.

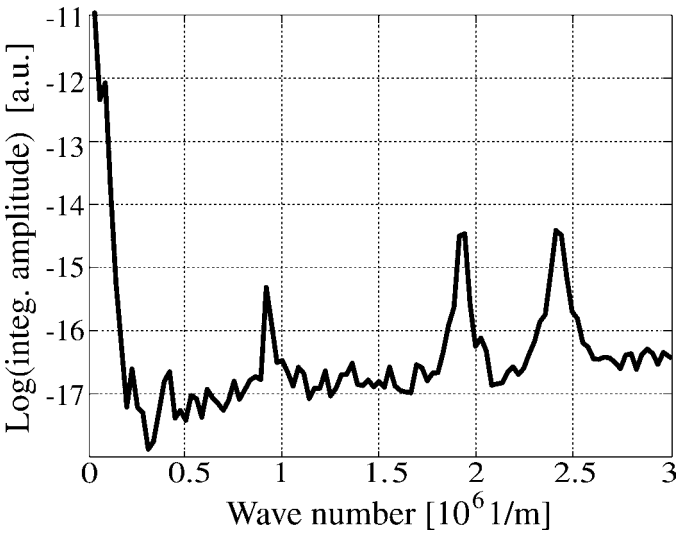

Fig. 9. Wavenumber spectrum obtained from the 2-D FFT of the measured vibration amplitudes at the frequency 1030 MHz through angular integration.

Due to the boundary conditions, a mode structure emerges that is described using dispersion curves. The dispersion curves indicate the wavenumbers (or phase velocities) and the frequencies at which the Lamb modes may propagate without attenuation[2]. Applying a suitable exci-

[2]For modes that propagate without damping in materials and without leakage of energy into the surrounding medium, the x-component of the wavevector (k_x) is real valued and the amplitude of the wave does not decay as it propagates.

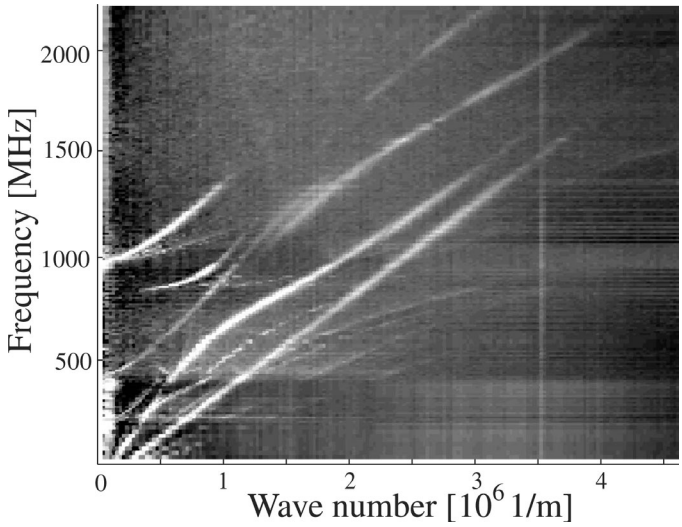

Fig. 10. Measured dispersion curves. Curves corresponding to the modes TS0, TE0, TS1, TS2, and TE1 clearly can be identified (see Fig. 11).

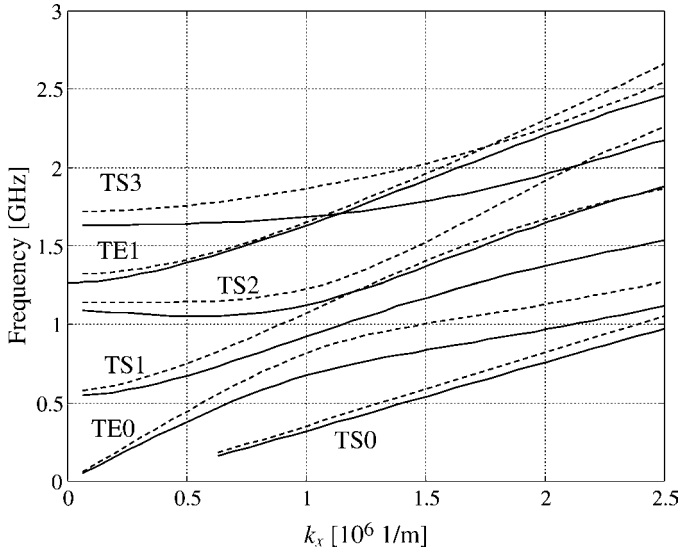

Fig. 11. Dispersion curves for the Lamb-wave modes in a ZnO plate. The solid curves are for the isotropic case, and the dashed curves are for the anisotropic, piezoelectric case.

tation (e.g., stress excitation through specifying the amplitude of one of the stress components at some interface), the frequencies of the propagating modes can be solved from the equations as functions of the lateral wavenumber.

For lossless modes, the mode frequencies are obtained as the frequencies at which a chosen field variable tends to infinity in response to the excitation (for given k_x).

The dispersion curves for Lamb-wave modes propagating in a laterally infinite 2.5 μm thick ZnO plate are plotted in Fig. 11. The number associated with the mode indicates the number of half-wavelengths in the thickness direction of the plate for the dominating displacement component of the mode, see Fig. 12. It is seen from Fig. 11 that there

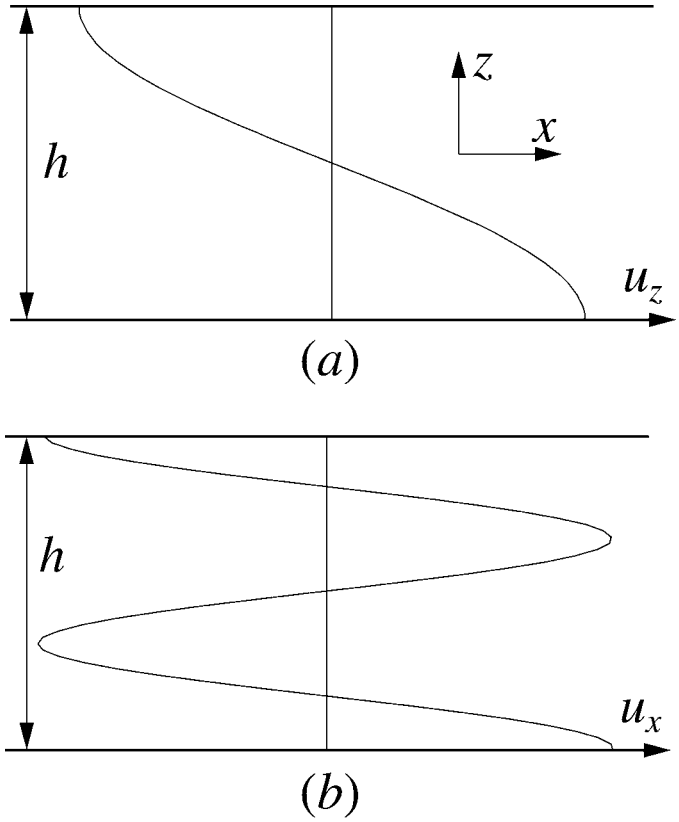

Fig. 12. Explanation of the nomenclature for the Lamb modes. (a) Displacement in the z-direction (u_z) for the fundamental TE1 mode. There is one half wavelength along the thickness direction. (b) Displacement in the x-direction (u_x) for the third thickness shear mode (TS3). There are three half wavelengths along the thickness direction. The thickness of the plate is denoted as h.

are considerable differences between the isotropic and the anisotropic, piezoelectric case. In the isotropic case, the relations between the ZnO materials constants are fixed like for an isotropic material, and their values are taken such that the density, the longitudinal bulk-wave velocity, and the shear bulk-wave velocity are close to those for real, physical ZnO (5687.2 kg/m^3, 6330 m/s and 2720 m/s, respectively). The differences between the two cases in Fig. 11 are mainly due to the anisotropy, the influence of piezoelectricity being weaker.

The modeled layer structure of SMR is shown in Fig. 1; it consists of a 370-nm thick Al top electrode, a 1882-nm thick ZnO, and a 395-nm thick Mo bottom electrode. Between the bottom electrode and the glass substrate, there are four mirror layers (from top to bottom): 1595-nm SiO_2, 1500-nm Mo, 1535-nm SiO_2, and 1575-nm Mo. In 1-D simulations, the thickness of the glass substrate is taken to be 701 μm; in the simulations of the dispersion curves, the glass substrate is modeled as a half-space.

The computed z-component of displacement is plotted in Fig. 13 as a function of the location within SMR at the resonance frequency (1114.1 MHz) associated with the TE1 mode. The displacements are computed using a 1-D model in which the field variables are taken to depend only on the z-coordinate. Weak attenuation is introduced

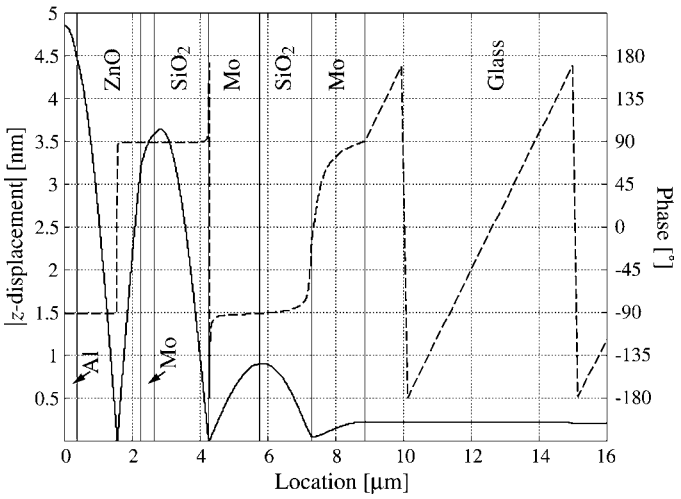

Fig. 13. Magnitude (solid line) and phase (dashed line) of the displacement component in the thickness (z) direction within the SMR at the series resonance frequency 1114.1 MHz of the TE1 mode computed with a 1-D model. The materials parameters for ZnO are taken from [14].

to the glass substrate in the simulation to avoid standing waves formed between the top surface of the stack and the bottom surface of the substrate; they would cause resonance peaks in the response that are closely spaced in frequency. The displacement plot indicates how the displacement amplitude of the TE1 mode decreases after each mirror layer and only a small fraction of the acoustic energy escapes into the substrate. However, the thicknesses of the mirror layers are slightly suboptimal, as the maximum of z-displacement does not occur exactly on the interface between the bottom electrode and the acoustic mirror.

Through increasing the number of layers in the mirror or by increasing the ratio between the acoustic impedances of the two materials used in the acoustic mirror, the acoustic energy leakage into the substrate may be further diminished. In addition, as a decreasing fraction of the total vibration energy will be contained in the acoustic mirror, the attainable effective coupling coefficient k_{eff} also increases with the ratio of the acoustic impedances [13].

V. Fitting Procedure

The materials parameters for film ZnO are determined through fitting, and those for the other materials are fixed. The objective function to be minimized in the fitting is:

$$\sum_{i=1}^{N}(f_{m,i} - f_{s,i})^2, \tag{3}$$

where N is the number of points on the measured dispersion curves used in the fitting ($N = 19$ was used); point i is on the measured dispersion curve at ($k_{x,i}$, $f_{m,i}$), and the corresponding point on the simulated dispersion curve is at ($k_{x,i}$, $f_{s,i}$). The points chosen for the fitting are identified

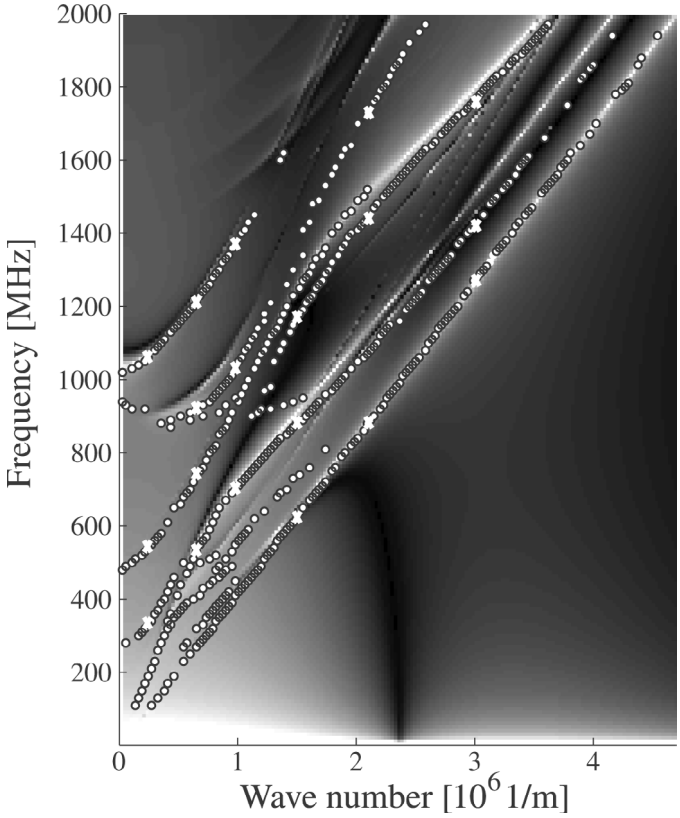

Fig. 14. Measured (circles) and simulated (grayscale) dispersion curves. The simulated curves have been obtained with the materials parameters in Table II. The crosses identify the points on the measured curves used in the fitting process.

with the crosses in Fig. 14; they have been selected only from those dispersion curves that clearly correspond to the TE and TS modes (see Fig. 11) in which the vibration energy is concentrated to the ZnO layer. The dispersion relations of these modes are expected to be sensitive to the materials parameters of ZnO and influence of other layers is expected to be reduced. There are additional insignificant peaks in the measured dispersion data (see Fig. 10), which are attributed to the properties of the FFT and to possible aliasing effects arising when interferometrically imaging waves featuring wavelengths smaller than the laser spotsize on the sample surface. These irrelevant peaks have been omitted.

To quantify the sensitivity of the dispersion curves to changes in the ZnO materials parameters, the magnitude of the relative change in frequency produced by a 3% increase of each ZnO materials constant was computed on 56 different points on the dispersion curves (for a Mo/ZnO/Al structure). Averaging over the 56 points for each materials constant, the values in Table I were obtained. It can be seen that the dispersion curves depend most strongly on the density and elastic constants of ZnO, and dependence on the piezoelectric and dielectric constants is an order of magnitude weaker. We conclude that the accuracy with which the piezoelectric and dielectric constants can be determined with the fitting procedure is correspondingly lower. Therefore, the piezoelectric and dielectric constants

TABLE I
MAGNITUDE OF RELATIVE CHANGE IN FREQUENCY AVERAGED OVER 56 SELECTED POINTS ON DISPERSION CURVES FOR 3% INCREASE IN THE MATERIALS CONSTANT.[1]

Materials constant	Frequency change [%]
Density	0.91
c_{11}	0.67
c_{12}	0.21
c_{13}	0.18
c_{33}	0.18
c_{44}	0.67
e_{33}	0.018
e_{31}	0.015
e_{15}	0.0094
ϵ_{11}	0.0095
ϵ_{33}	0.017

[1]Computed for Mo/ZnO/Al structure.

are fixed in the optimization to the values for single-crystal ZnO taken from [14] and only the values of the density and the elastic constants of ZnO are optimized.

In the optimization, a conjugate-gradient minimizer with the Polak-Ribiere update rule [15] was used. To verify the method, it was first tested for a simpler layer stack consisting of a Mo bottom electrode, ZnO film, and Al top electrode. The dispersion curves for this structure were computed using published values for the materials constants. Points on these computed dispersion curves were used to replace the measured values in (3). Then, several optimizations with different starting values for the density and elastic constants were carried out. The starting values were obtained through randomly varying the published values by ±20%. The optimization process consistently provided results close to the published values. The difference between the optimized and published values of the density and elastic constants for ZnO decreased as N in (3) increased and as the number of modes on whose dispersion curves the points were chosen was increased.

The optimization procedure described above was carried out for the mirror resonator structure in Fig. 1. The optimization was run 400 times, and, at the start of each optimization loop, the density and the elastic constants of ZnO were randomly varied ±20% from their bulk values. From the different sets of materials parameters that yield a fair matching result, the one for which the density is not too far above the bulk value (as materials in thin-film form are less dense than in bulk crystalline form) and for which the TE1 frequency for $k_x = 0$ is close to the measured value was chosen as the best-fit result, listed in Table II. Note that the materials parameters given should not be considered as absolutely accurate but as only indicative since the materials parameters of the electrodes and mirror layers also somewhat affect the dispersion curves. In addition, the temperature of the resonator can rise during the laser-probe measurement owing to the relatively high-input power that is fed into the resonator. However, our measurements indicate that the temperature elevation is practically insignificant, e.g., at the TE1 resonance with a 14-dBm input power it is below 10°C.

TABLE II
DENSITY AND ELASTIC CONSTANTS OBTAINED FOR FILM ZNO THROUGH FITTING THE SIMULATED AND MEASURED DISPERSION CURVES.

Materials constant	Best-fit value	Bulk value [14]	Difference [%]
Density (kg/m^3)	5837	5700	2.4
c_{11} (GPa)	184.6	210	−12.1
c_{12} (GPa)	123.3	121	1.9
c_{13} (GPa)	95.3	105	−9.3
c_{33} (GPa)	174.1	211	−17.5
c_{44} (GPa)	34.8	43	−19.1

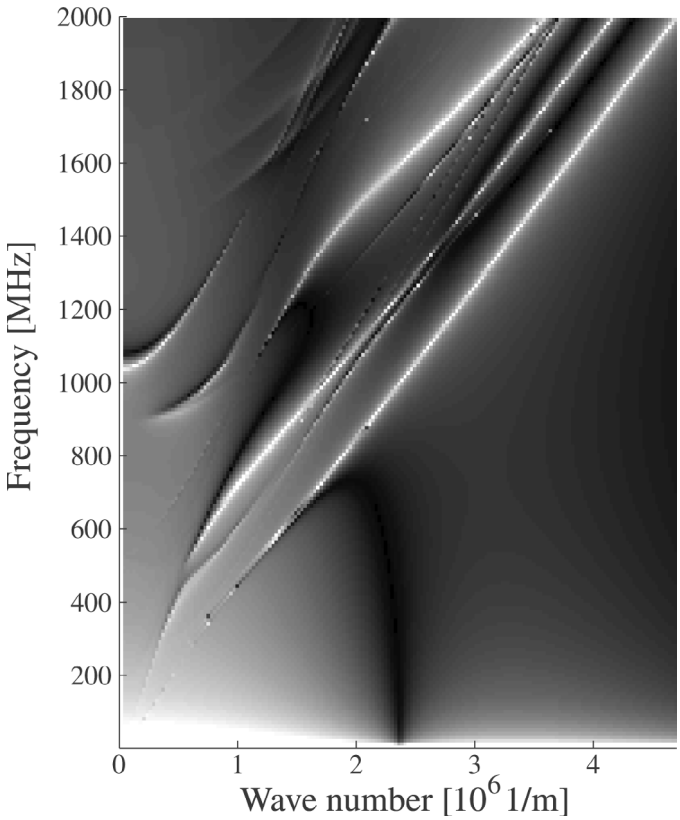

Fig. 15. Simulated dispersion curves obtained with the materials parameters in Table II. In the simulations, the excitation is through the stress T_{zz} at the top surface of the stack, and the response (plotted with shades of gray) is the z-displacement (vibration amplitude u_z) at the top surface of the stack.

The dispersion curves simulated using the optimized materials parameters for ZnO are shown in Fig. 15. Note that the simulation also predicts the strengths of the measured dispersion curves reasonably well, as can be judged by comparing Figs. 10 and 15. The sole loss mechanism included in the model is the radiation of the acoustic energy into the substrate. However, in the measurements there are other factors affecting the amplitudes and shapes of the curves, e.g., the power delivered to the resonator de-

pends on frequency. The measured dispersion curves together with the simulated curves are compared in Fig. 14. It can be observed that they agree fairly well.

VI. Conclusions

An approach of fitting the simulated dispersion curves with the experimental dispersion curves obtained interferometrically from thin-film bulk resonators to determine the properties of thin films has been presented. Although the measured and simulated dispersion curves agree fairly well, the accuracy and reliability of the materials parameters evaluated with the technique used is somewhat reduced for the complex layer structure considered here, because of the lack of a one-to-one mapping between the materials parameters and the dispersion relations. It also was found that the values of the piezoelectric and dielectric constants for ZnO only weakly affect the dispersion behavior; consequently, they are difficult to determine accurately using the present method. The materials constants vary between different fitted sets of materials parameters (which result in an object function value close to the minimum). A set of parameters with density close to the bulk value and fundamental TE1 frequency close to the measured value is considered as the most reliable set.

An additional complication may arise from the fact that, in the simulations, the materials properties are considered to be homogeneous; although in the actual measured resonators the properties of the ZnO may vary close to the bottom electrode in which the ZnO deposition starts, as compared to the properties farther away from the interface [16]. It also is assumed in the simulations that the ZnO is strictly c-axis oriented. Considering the difficulty of an accurate and complete characterization of the properties of materials in thin-film form, the technique described above can serve to complement other methods used for estimations of the materials parameters. A benefit of our approach is that no special test structures [17] are required for the evaluation of the materials parameters; however, for that purpose one may use the very same resonators used to constitute, e.g., bandpass filters [18], [19]. However, it is expected that through using specialized test structures suitable for precise measurements, the results can be further improved.

For the SMR structure considered, accuracy of the fitted materials parameters requires that the layer thicknesses of the many layers in the stack are known precisely. In principle, the method could be used to obtain the materials parameters for several thin-film materials in the stratified structure simultaneously. To determine the properties of only the piezoelectric layer using the present method, it would be advantageous to use a membrane-type thin-film BAW resonator in the measurements, consisting of a piezoelectric material between thin electrodes and possibly a support layer of, e.g., silicon. However, the bending of the membrane structure due to possible residual stresses in the films renders its fabrication [20], as well as its interferometric imaging, more challenging. In general, the less layers there are, the simpler and more reliable the fitting procedure becomes.

Acknowledgments

The authors thank Dr. J. Koskela for creating the first versions of the simulation software and O. Holmgren, Helsinki University of Technology (HUT) for carrying out the laser-interferometric measurements. We also are grateful to Dr. M. Ylilammi (VTT, Technical Research Centre of Finland), J. Ellä, (Nokia Mobile Phones [NMP]), I. Suni (VTT), H. Pohjonen (NMP), and Prof. V. P. Plessky for valuable advice and inspiring discussions.

References

[1] T. W. Grudkowski, J. F. Black, T. M. Reeder, D. E. Cullen, and R. A. Wagner, "Fundamental-mode VHF/UHF miniature acoustic resonators and filters on silicon," *Appl. Phys. Lett.*, vol. 37, no. 11, pp. 993–995, 1980.

[2] K. M. Lakin and J. S. Wang, "Acoustic bulk wave composite resonators," *Appl. Phys. Lett.*, vol. 38, no. 3, pp. 125–127, 1981.

[3] P. Bradley, R. Ruby, J. D. Larson, III, Y. Oshmyansky, and D. Figueredo, "A film bulk acoustic resonator (FBAR) duplexer for USPCS handset applications," *IEEE MTT-S Dig.*, vol. 1, pp. 367–370, 2001.

[4] R. F. Milsom, "Two-dimensional theory of thin-film ZnO resonators on silicon," in *Proc. IEEE Ultrason. Symp.*, 1982, pp. 484–489.

[5] J. E. Graebner, H. F. Safar, B. Barber, P. L. Gammel, J. Herbsommer, L. A. Fetter, J. Pastalan, H. A. Huggins, and R. E. Miller, "Optical mapping of surface vibrations on a thin-film resonator near 2 GHz," in *Proc. IEEE Ultrason. Symp.*, 2000, pp. 635–638.

[6] G. G. Fattinger and P. T. Tikka, "Laser measurements and simulations of FBAR dispersion relation," in *Proc. IEEE MTT-S Int. Microwave Symp.*, 2001, pp. 371–374.

[7] D. Royer and E. Dieulesaint, *Elastic Waves in Solids I.* Berlin: Springer-Verlag, 2000.

[8] K. Nakamura, Y. Ohashi, and H. Shimizu, "UHF bulk-acoustic-wave filters utilizing thin ZnO/SiO_2-diaphragms on silicon," *Jpn. J. Appl. Phys.*, vol. 25, pp. 371–375, 1986.

[9] G. G. Fattinger and P. T. Tikka, "Modified Mach-Zehnder laser interferometer for probing bulk acoustic waves," *Appl. Phys. Lett.*, vol. 79, no. 3, pp. 290–292, 2001.

[10] J. T. Stewart and Y.-K. Yong, "Exact analysis of the propagation of acoustic waves in multilayered anisotropic piezoelectric plates," *IEEE Trans. Ultrason., Ferroelect., Freq. Contr.*, vol. 41, no. 3, pp. 375–390, 1994.

[11] M. J. Lowe, "Matrix techniques for modeling ultrasonic waves in multilayered media," *IEEE Trans. Ultrason., Ferroelect., Freq. Contr.*, vol. 42, no. 4, pp. 525–542, 1995.

[12] T. Pastureaud, V. Laude, and S. Ballandras, "Stable scattering-matrix method for surface acoustic waves in piezoelectric multilayers," *Appl. Phys. Lett.*, vol. 80, no. 14, pp. 2544–2546, 2002.

[13] K. Nakamura and H. Kobayashi, "Thin film resonators and filters," in *Int. Symp. Acoust. Wave Devices for Future Mobile Commun. Syst.*, 2001, pp. 93–99.

[14] J. F. Rosenbaum, *Bulk Acoustic Wave Theory and Devices.* Boston: Artech House, 1988.

[15] W. H. Press, S. A. Teukolsky, W. T. Vetterling, and B. P. Flannery, *Numerical Recipes in C: The Art of Scientific Computing.* 2nd ed. Cambridge: Cambridge University Press, 1992.

[16] G. Carlotti, D. Fioretto, L. Palmieri, G. Socino, L. Verdini, and E. Verona, "Brillouin scattering by surface acoustic modes for elastic characterization of ZnO films," *IEEE Trans. Ultrason., Ferroelect., Freq. Contr.*, vol. 38, no. 1, pp. 56–61, 1991.

[17] R. S. Wagers, "PVF_2 elastic constants evaluation," in *Proc. IEEE Ultrason. Symp.*, 1980, pp. 464–469.
[18] J. Kaitila, M. Ylilammi, J. Molarius, J. Ellä, and T. Makkonen, "ZnO based thin film bulk acoustic wave filters for EGSM band," in *Proc. IEEE Ultrason. Symp.*, 2001, pp. 803–806.
[19] M. Ylilammi, J. Ellä, M. Partanen, and J. Kaitila, "Thin film bulk acoustic wave filter," *IEEE Trans. Ultrason., Ferroelect., Freq. Contr.*, vol. 49, no. 4, pp. 535–539, 2002.
[20] R. Lanz, P. Carazzetti, and P. Muralt, "Surface micromachined BAW resonators based on AlN," in *Proc. IEEE Ultrason. Symp.*, 2002, pp. 956–958.

Tapani Makkonen (M'98) was born in Helsinki, Finland in 1968. He received the M.Sc. and the Lic.Tech. degrees in engineering physics from the Helsinki University of Technology in 1996 and 2001, respectively. Presently, he is working at the Materials Physics Laboratory towards his Ph.D. His research interests include modeling of SAW and BAW physics and devices. Mr. Makkonen is a member of the Finnish Physical Society. He is a corecipient of the UFFC Society 2001 Outstanding Paper Award.

Tuomas Pensala was born in Helsinki, Finland in 1972. He received the M.Sc. degree in engineering physics from the Helsinki University of Technology in October 2000. He works as a research scientist at VTT Technical Research Centre of Finland, where he has been since 1998. His research interests include fabrication, design and modelling of thin film BAW devices.

Juha Vartiainen was born in Jämsä, Finland in 1978. He received the M.Sc. degree in engineering physics from the Helsinki University of Technology (HUT) in 2002. He is a postgraduate student in the Materials Physics Laboratory at HUT. His research interests include theoretical materials physics and optical imaging of surface waves.

Jouni V. Knuuttila was born in Marttila, Finland in 1972. He received the M.Sc. degree in engineering physics from Helsinki University of technology (HUT) in 1998. He is a postgraduate student in the Materials Physics Laboratory at HUT. His research interests include optical imaging of surface and bulk acoustic waves, sonoluminescence and audio signal processing. He is a member of the Finnish Optical Society. Mr. Knuuttila is a corecipient of the UFFC Society 2001 Outstanding Paper Award.

Jyrki Kaitila was born in Helsingin mlk., Finland in 1966. He received the degrees of M.Sc. in engineering physics and Lic.Tech. in electrical engineering from the Helsinki University of Technology in 1994 and 1996, respectively. Since 1995 he has worked at VTT Technical Research Centre of Finland. His current research interests include physics and manufacturing technology of FBAR devices.

Martti M. Salomaa (M'95) received his Dr.Tech. degree in technical physics from Helsinki University of Technology (HUT) in 1979. Thereafter, he worked at UCLA and the University of Virginia. From 1982 to 1991, he was the theory group leader at the Low Temperature Laboratory, HUT, and from 1988 to 1991, he served as Director of the ROTA project between the Academy of Finland and the Soviet Academy of Sciences. He has held a sabbatical stipend at the University of Karlsruhe, and, in 1994, he was Guest Professor at ETH-Zürich. Since 1996, he has been a professor of technical physics and the Director of the Materials Physics Laboratory in the Department of Technical Physics and Mathematics at HUT. He is a corecipient of the 1987 Award for the Advancement of European Science (presented by the Körber Foundation, Hamburg). His research interests include superfluidity, superconductivity, magnetism, physics of SAW, nondiffracting waves, and mesoscopic physics. He is a member of the IEEE, APS, EPS, and the Finnish Physical